



Article

Spatial Assessment of Nitrogen Dioxide (NO₂) in Lithuania's Coastal Zones: A Remote Sensing Approach for Sustainable Urban Planning

Aistė Andriulė^{1,*} , Erika Vasiliauskienė^{1,2}, Remigijus Dailidė¹  and Inga Dailidienė^{1,3}

¹ Marine Research Institute, Klaipėda University, H. Manto Str. 84, 92294 Klaipėda, Lithuania; erika.vasiliauskienė@ku.lt (E.V.); remigijus.dailidė@gmail.com (R.D.); inga.dailidienė@ku.lt (I.D.)

² Business Faculty, Klaipėdos Valstybinė Kolegija/Higher Education Institution, 91274 Klaipėda, Lithuania

³ Technology Department, Lithuanian Business College, 91249 Klaipėda, Lithuania

* Correspondence: aiste.andriule@ku.lt; Tel.: +370-64145744

Abstract

Nitrogen dioxide (NO₂) is a short-lived atmospheric pollutant primarily emitted by road traffic, maritime shipping, and industrial combustion. It is a key indicator of anthropogenic air pollution due to its harmful health effects, its role in the formation of secondary particulate matter, and its strong association with other traffic-related pollutants. Elevated NO₂ concentrations are closely linked to respiratory and cardiovascular diseases, with children and elderly populations being particularly vulnerable due to physiological susceptibility and exposure patterns. This study uses satellite-based remote sensing data to assess the spatial and temporal variability of NO₂ concentrations in the Lithuanian coastal zone and adjacent marine areas. The analysis focuses on identifying spatial patterns of NO₂ concentration distribution, localized pollution hotspots, and their relationships with population distribution. Correlation analysis for the 2022–2024 period revealed a statistically significant negative relationship between NO₂ concentrations and distance from the coastline in inland areas, whereas no statistically significant relationship was observed offshore. NO₂ concentrations at 0 m and 50 m were strongly positively correlated across all spatial domains and seasons ($r > 0.98$, $p < 0.001$), indicating consistent vertical spatial patterns. Annual mean NO₂ concentrations were also strongly positively associated with population density ($r = 0.81$).

Keywords: nitrogen dioxide; remote sensing; sustainability; urban planning



Academic Editor: Ana Cláudia Teodoro

Received: 1 February 2026

Revised: 10 March 2026

Accepted: 12 March 2026

Published: 13 March 2026

Copyright: © 2026 by the authors.

Licensee MDPI, Basel, Switzerland.

This article is an open access article distributed under the terms and

conditions of the [Creative Commons](https://creativecommons.org/licenses/by/4.0/)

[Attribution \(CC BY\)](https://creativecommons.org/licenses/by/4.0/) license.

1. Introduction

Nitrogen dioxide (NO₂) is a major atmospheric pollutant in urban environments, with road traffic recognized as its dominant source in most cities. NO₂ is primarily emitted from vehicle exhaust, particularly in areas with high traffic density, and has been widely used as a key indicator of traffic-related air pollution [1]. Additional sources include fossil fuel combustion in industrial processes and residential heating, as well as secondary atmospheric formation through photochemical reactions. Nitrogen dioxide (NO₂) plays a critical role in the formation of tropospheric ozone and secondary particulate matter, both of which contribute to regional air quality degradation [2,3]. Long-term exposure to NO₂ has been linked to a range of adverse health outcomes, including respiratory and cardiovascular diseases, impaired lung function, and increased premature mortality, particularly in densely populated urban settings [4]. These impacts underscore the importance of detailed

spatial analyses of NO₂ distribution to inform effective environmental health and policy responses. For regulatory and health context, NO₂ reference thresholds are commonly expressed as mass concentrations ($\mu\text{g}/\text{m}^3$), such as the EU annual limit value ($40 \mu\text{g}/\text{m}^3$) and hourly limit value ($200 \mu\text{g}/\text{m}^3$, with a limited number of allowed exceedances), while the 2021 WHO Air Quality Guidelines recommend lower levels ($10 \mu\text{g}/\text{m}^3$ annual mean and $25 \mu\text{g}/\text{m}^3$ 24-h mean). These values are provided as contextual benchmarks, although NO₂ in this study is reported in parts per million by volume (ppmv) because a gridded remote-sensing (satellite-based) data product is used. Such technologies, together with recent advances in satellite air-pollution monitoring, make it possible to assess NO₂ spatial patterns regularly over large areas and at sufficiently detailed spatial resolution.

Recent advances in satellite remote sensing have significantly enhanced the monitoring of nitrogen dioxide (NO₂), enabling detailed spatial and temporal analyses of pollutant concentrations across urban, industrial, and coastal environments. A key development was the launch of the Sentinel-5 Precursor (Sentinel-5P) satellite in October 2017, which carries the Tropospheric Monitoring Instrument (TROPOMI)—currently the most advanced satellite instrument for measuring tropospheric NO₂. TROPOMI provides near-global daily coverage with a spatial resolution of $3.5 \times 7 \text{ km}^2$ at launch, later improved to $3.5 \times 5.5 \text{ km}^2$, offering unprecedented detail for urban-scale air quality studies [5].

Its predecessor, the Ozone Monitoring Instrument (OMI), launched in 2004 aboard NASA's Aura satellite, had a coarser spatial resolution of approximately $13 \times 24 \text{ km}^2$, which limited its capacity to resolve localized emission sources in heterogeneous environments [6]. By contrast, TROPOMI, onboard Sentinel-5P since 2017, offers daily global coverage at much finer resolution ($\sim 3.5 \times 5.5 \text{ km}^2$ as of 2019), enabling detailed identification of NO₂ hotspots. Although pixel sizes increase with latitude due to geometric distortion—reaching over 6 km in width at $\sim 55^\circ \text{ N}$ (Lithuania)—TROPOMI remains vastly superior for regional NO₂ monitoring [7]. Its high spatial resolution has also significantly improved the performance of integrated air quality systems such as the Copernicus Atmosphere Monitoring Service (CAMS), which assimilates satellite data with ground-based observations to produce spatially consistent atmospheric composition fields.

Building on these capabilities, recent studies in Europe have extensively examined the spatial distribution of nitrogen dioxide (NO₂) in major coastal urban areas using high-resolution satellite data. These studies have revealed distinct NO₂ concentration patterns associated with urban density, industrial activity, and port operations, such as in Paris and Mediterranean port cities [7,8]. However, significantly less attention has been directed toward smaller or medium-sized coastal urban centers—such as Klaipėda in Lithuania—despite their growing economic and logistical roles.

Klaipėda, Lithuania's only seaport, serves as a key industrial, transport, and urban hub on the eastern Baltic coast. Recognized as the most diversified and strategically important port in the region [9], it is also the most populous and industrialized settlement along the Lithuanian shoreline, playing a central role in shaping the environmental profile of western Lithuania. Although smaller in scale than major European ports, Klaipėda faces comparable environmental pressures, including high freight intensity, residential areas in close proximity to industrial infrastructure, and a heating season lasting over half the year.

The broader Lithuanian coastal region encompasses a mix of land use types—from dense urban zones and resort towns like Palanga to rural settlements and protected areas along the Curonian Spit. While emission sources vary, nitrogen dioxide (NO₂) pollution across this zone is primarily driven by road traffic and industrial activity, with localized contributions from port operations and residential energy use in non-urban areas [1]. Despite this diverse emission landscape, high-resolution spatial assessments of NO₂ distribution

remain scarce in the Lithuanian context, especially in comparison to well-studied Western European coastal regions.

This study addresses this gap by analyzing the spatial and seasonal distribution of NO₂ in Klaipėda and its surrounding coastal region between 2022 and 2024. Using satellite-based measurements from TROPOMI and a grid-based spatial framework, we examine how NO₂ concentrations vary with distance from the shoreline, between two vertical levels (0 m and 50 m), and across different seasons. In addition, we assess how pollutant concentrations correspond with population distribution across the coastal belt, clarifying the spatial link between anthropogenic pressure and NO₂ levels, and supporting more informed spatial planning decisions. Although similar studies have been conducted in larger Western European port regions, this research provides the first high-resolution spatial assessment of NO₂ distribution along the Lithuanian coast. The findings contribute to a more geographically balanced understanding of coastal air pollution dynamics in the southeastern Baltic Sea region and offer a foundation for future regional air quality analysis and planning efforts.

2. Materials and Methods

2.1. Study Area

The study area (Figure 1) encompasses the westernmost part of Lithuania and its adjacent territorial waters in the Baltic Sea. The terrestrial domain includes five municipalities: Klaipėda City, Klaipėda District, Palanga City, Neringa Municipality, and Kretinga District, covering a total area of approximately 3750 km² [10]. Geographically, the region borders the Republic of Latvia to the north, the Kaliningrad Oblast of the Russian Federation to the south, and stretches westward along the entire Lithuanian coastline of the Baltic Sea. To better understand the geographic scope of the analysis, including both land-based and marine domains, the study area is depicted in Figure 1.

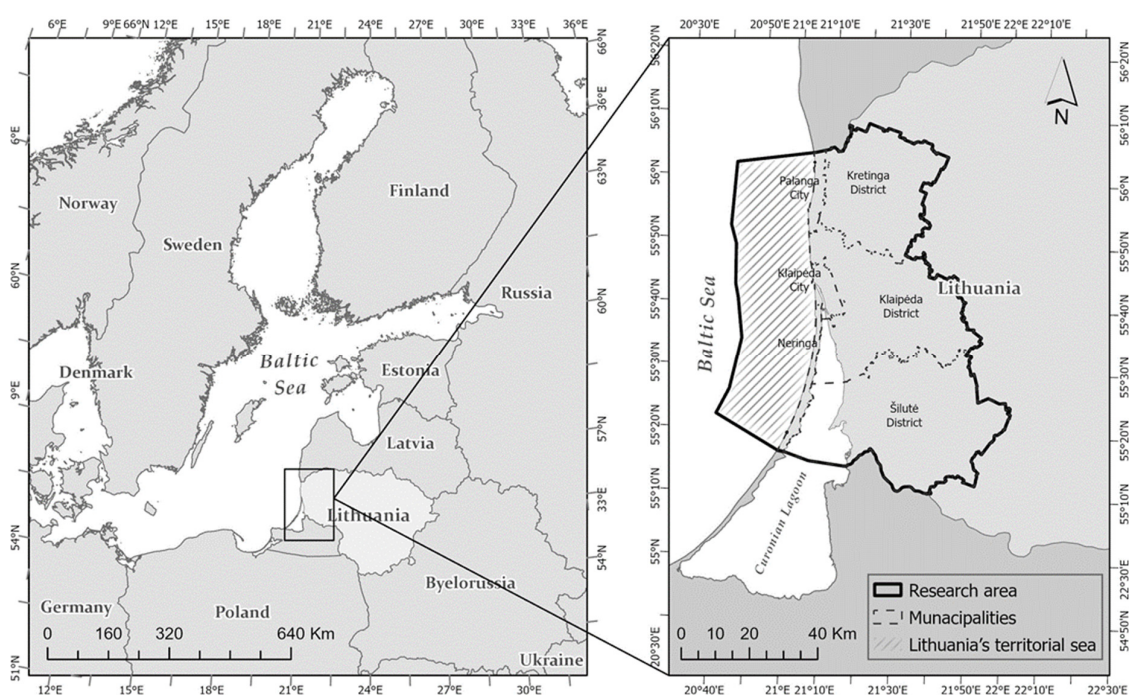


Figure 1. The study area: South East Baltic Sea region, covering western Lithuania and its adjacent territorial waters.

The length of Lithuania's Baltic Sea coastline is approximately 98 km [11]. It consists of the mainland coastal strip between Palanga and Klaipėda, as well as the Curonian Spit, a

narrow, ~98 km-long sand barrier separating the Curonian Lagoon from the open sea. This coastal zone is characterized by diverse morphology, including sandy beaches, foredunes, dune ridges, and lagoon-type shores. These land–sea interface areas are sensitive to both natural dynamics and anthropogenic pressures, such as tourism, port activities, and coastal erosion [11].

A distinctive feature of the region is the Curonian Lagoon, a large, shallow transitional inland water body primarily fed by freshwater inflow from the Nemunas River basin. Although hydrologically connected to the Baltic Sea via the Klaipėda Strait, the lagoon has limited exchange with the sea, resulting in predominantly inland hydrological processes. For this reason, it is classified as a transitional inland water body [12]. Accordingly, in this study, areas located within the lagoon are considered part of the land (inland) domain. While navigation occurs in the Curonian Lagoon, it is primarily used for inland waterway transport and regional connections, with limited suitability for international maritime shipping due to shallow depth and infrastructural constraints [13].

The study area is dominated by a coastal lowland, with limited topographic variation. In such open, low-relief landscapes, air pollutant dispersion tends to be more uniform and more predictable compared to complex terrain, where local features may disturb airflow and result in spatial concentration variability [14].

Climatically, Western Lithuania is influenced by both maritime and continental air masses. The coastal zone exhibits a distinct mesoclimatic regime, shaped by the sea: seasonal temperature variation is reduced, relative humidity is higher, wind intensity is greater, and sea breeze circulation is more frequent [15]. Further inland, the climate becomes increasingly continental, with more pronounced daily and annual temperature fluctuations. This land–sea climatic gradient, combined with the uniform relief of the coastal lowland, creates favorable conditions for analyzing air pollution distribution and atmospheric transport processes. Compared to topographically complex areas, modeling atmospheric dispersion in such open landscapes yields more accurate results with lower risk of local-scale uncertainties [16].

The marine part of the study area includes Lithuania's territorial waters, which extend up to 12 nautical miles (approximately 22.2 km) from the coastline, covering an area of around 6400 km² [11]. This section of the sea belongs to the southeastern Baltic Proper and is characterized by low salinity, weak tidal influence, and shallow coastal bathymetry. Territorial waters play a significant role in the regional economy—supporting commercial and recreational fisheries, maritime navigation, and coastal tourism—and are partially included in protected zones [17].

2.2. Data and Methods

The analysis employed a gridded spatial framework based on the Copernicus Atmosphere Monitoring Service (CAMS; operated by the European Centre for Medium-Range Weather Forecasts, UK) data system. CAMS provides model-based atmospheric composition fields generated by assimilating multiple observational sources through the European Centre for Medium-Range Weather Forecasts (ECMWF) Integrated Forecasting System. Specifically, the Copernicus Atmosphere Monitoring Service Global Anthropogenic Emissions Inventory (CAMS-GLOB-ANT v4.2) integrates satellite-based tropospheric NO₂ retrievals from the Tropospheric Monitoring Instrument (TROPOMI) on Sentinel-5P, the Ozone Monitoring Instrument (OMI) on Aura, and the Global Ozone Monitoring Experiment-2 (GOME-2) on MetOp, as well as in situ surface measurements and complementary global inventories, to produce consistent, quality-controlled emission fields on a global scale [18,19].

In this study, these capabilities were utilized to extract harmonized NO₂ emission fields over the Lithuanian coastal region. The NO₂ emissions data used in this study were obtained from CAMS-GLOB-ANT v4.2, which provides monthly average values on a regular 0.1° × 0.1° spatial grid [18]. At the latitude of Lithuania (~55° N), this resolution corresponds approximately to 11.1 km in the north–south direction and 6.2 km in the east–west direction, enabling consistent and spatially harmonized air quality analysis along the coastline. The dataset covers multiple years; however, this study focused on the period 2022–2024. Although data for 2021 were initially extracted, they were excluded from the analysis due to detected inconsistencies in grid alignment and spatial shifts that compromised comparability with later years.

The CAMS European air-quality reanalysis is produced using an ensemble of eleven data-assimilation modelling systems; an ensemble median is provided, and the inter-model spread can be used as an estimate of analysis uncertainty. Because the NO₂ fields used here come from a gridded reanalysis product rather than direct sensor measurements, a single instrument detection limit is not directly applicable. Meteorological conditions are an additional source of uncertainty for NO₂ estimates, as they modulate dispersion, mixing, and the quality of remote-sensing retrievals. In particular, relative humidity may influence the precision of NO₂ retrievals indirectly through its effects on cloud formation, aerosol optical behaviour, and boundary-layer dynamics. Therefore, auxiliary meteorological variables and cloud screening procedures are incorporated within the retrieval/assimilation framework, although some residual uncertainty may remain under certain atmospheric conditions. Accordingly, the results are interpreted primarily as spatial gradients and relative differences across the study area rather than exact point-level concentrations.

CAMS data were processed in ArcGIS Pro v3.xx (Esri, Redlands, CA, USA) to extract monthly mean NO₂ values for the period 2022–2024 and ensure consistent spatial coverage across the study area. NO₂ concentration values—originally expressed in parts per million by volume (ppmv)—were extracted from the CAMS gridded dataset using GIS-based techniques. Each grid cell was represented by a centroid, and the geographic coordinates of these centroids were used to retrieve monthly mean NO₂ values from the dataset. This centroid-based extraction method is commonly used in satellite air pollution studies to ensure consistency across grid structures, particularly when polygon shapefiles of grid boundaries are unavailable [20,21]. To ensure full spatial coverage along the Lithuanian coastline and to avoid excluding relevant grid cells whose centroids fall just outside the designated study area, a 5 km buffer zone was applied. This allowed for the inclusion of grid cells whose spatial footprint still overlapped substantially with the analysis region. Such buffering techniques are frequently applied in air pollution mapping studies to reduce edge effects and improve spatial completeness, especially in coastal and irregular regions [22]. The resulting spatial framework—showing the extent of the 0.1° × 0.1° grid and the applied 5 km study area buffer—is illustrated in Figure 2.

Figure 2 provides a visual representation of the spatial grid layout, the applied 5 km buffer zone, and the alphanumeric indexing system used to classify and reference each grid cell within the study area, serving as a spatial reference for the analytical zones. Spatial grid indexing is a widely applied method in geographic information science to facilitate analytical consistency, zonal classification, and comparative spatial referencing [23].

Based on this framework, each grid cell was assigned to one of three spatial domains according to its geographic overlap with land and sea: offshore, inland, or coastal transition. Offshore grid cells were located entirely within the Baltic Sea, inland grid cells lay fully on land, and coastal transition grid cells were situated along the irregular shoreline, representing the interface between terrestrial and marine environments. These domains were

systematically differentiated through the alphanumeric indexing scheme, which supported clear spatial classification and data extraction throughout the study.

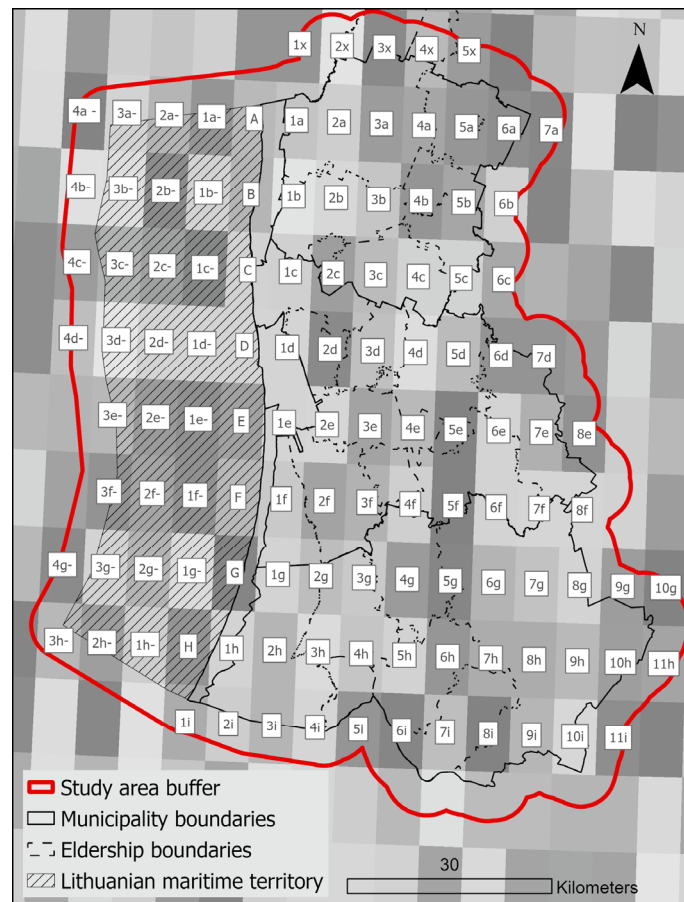


Figure 2. CAMS gridded framework and assigned cell indices across the Lithuanian coastal study area, with a 5 km buffer applied. Note: Spatial grid framework of the study area with a 5 km buffer. Alphanumeric labels indicate grid-cell identifiers: numbers and lowercase letters denote the cell index, uppercase letters indicate coastal transition zones, and the trailing hyphen in labels such as 1a- marks maritime/offshore cells.

Grid cells that directly overlapped both land and sea were designated as coastal transition grid cells and labeled using single capital letters (A–H), corresponding to their coastal zone. These grid cells did not receive numeric distance classes, as they represented transitional land–sea interface zones. Grid cells A through G generally followed a near-linear progression along the coast, maintaining consistent longitudinal alignment between the inland, coastal transition, and offshore domains. However, in the southern part of the study area, the coastline curves sharply westward along the Curonian Spit, requiring a spatial adjustment. To preserve logical alignment within this zone, grid cell H was shifted westward to follow the shoreline’s curvature while remaining aligned with its adjacent inland and offshore counterparts. Although water-covered, the Curonian Lagoon was classified as part of the inland domain, as it constitutes a semi-enclosed brackish water body that is both hydrologically and ecologically distinct from the open Baltic Sea. Furthermore, under international maritime law, such lagoons are typically designated as internal waters rather than part of the territorial sea or open ocean [24].

The numeric component (1 to 6) denoted the grid cell’s distance class from the coastline (in 6.2 km increments, based on grid width), while the lowercase letter component (“a” to “i” inland and “a” to “h” offshore) indicated horizontal alignment with the corresponding

coastal transition grid cell. An optional trailing dash (–) was used to designate offshore grid cells. For example, “3a–” refers to a third-distance-class offshore cell aligned with coastal zone A, whereas “3a” is its inland counterpart. In line with the established spatial classification logic, cells labeled as “x” were not integrated into the inland–coastal–offshore alignment and were consequently excluded from analysis.

The implementation of a structured spatial indexing system enabled three levels of quantitative analysis across the study area, each targeting a distinct dimension of NO₂ spatial variation:

- i. horizontal concentration gradients with increasing distance from the coastline.

Pearson’s correlation coefficient (r) was used to quantify linear associations between predefined distance classes and mean NO₂ concentrations. Pearson’s correlation coefficient (r) is widely employed in environmental and geographic research for assessing spatial relationships between variables such as pollutant concentrations, land-use metrics, or meteorological factors [25]. The analysis was conducted separately for each of the two vertical levels (0 m and 50 m), and for each year (2022, 2023, and 2024), within both inland and offshore domains. An additional multi-year average (2022–2024) was calculated for each grid cell and used to assess aggregated trends over the entire study period. To ensure comparability between the inland and offshore domains, two sampling strategies were implemented: (1) the full inland dataset ($n = 71$) was compared with the complete offshore dataset ($n = 32$) to capture broad domain-level contrasts; (2) the size-matched inland subsample ($n = 32$) was constructed to mirror the offshore domain. This inland subset consisted of four grid cells selected from each of the eight horizontal sectors (a–h), within distance classes 1 to 4 (8 sectors \times 4 distances = 32 grid cells). This structured sampling approach avoided random selection and ensured spatial balance across the inland gradient. The coastal transition zone ($n = 8$), consisting of grid cells overlapping both land and sea, was excluded from this analysis due to its hybrid environmental character and limited sample size.

- ii. vertical structure and seasonal dynamics of NO₂ between surface (0 m) and elevated (50 m) levels.

Vertical gradients in NO₂ concentrations were assessed using paired measurements at two altitudes—0 m and 50 m—across three spatial domains: inland ($n = 71$), coastal transition zone ($n = 8$), and offshore ($n = 32$). These altitudes were selected to characterize vertical stratification and mixing within the lower atmosphere, where concentration differences are sensitive to changes in stability, turbulence, and local emission influences. To address differences in station density across domains, a reduced inland subset ($n = 32$) was created by spatially thinning the inland network to match the offshore grid resolution. This allowed for a more balanced comparison of vertical gradients across domains with different spatial coverage.

Vertical NO₂ differences (Δ [50 m – 0 m]) were calculated at the grid-cell level based on 2022–2024 data. For each domain and season, the Δ values from all valid grid cells were averaged to compute a domain-level seasonal mean. This approach ensured equal spatial weighting and avoided biases due to uneven station distributions.

To evaluate the magnitude and robustness of the vertical gradients, arithmetic means, 95% confidence intervals (CIs), and standardized effect sizes (Cohen’s d_z) were calculated. Cohen’s d_z is commonly used in environmental studies involving repeated or paired measurements, providing an interpretable measure of practical significance when comparing values at two levels within the same location [26]. Confidence intervals were used to quantify the precision of estimated differences, as recommended in environmental science for transparency and reproducibility [27].

To further assess the coherence of vertical profiles, Pearson correlation coefficients (r) were calculated between NO_2 concentrations at 0 m and 50 m, using seasonal mean values per grid cell. This metric allowed evaluation of whether both heights responded similarly to regional emission patterns and atmospheric drivers.

iii. spatial associations between surface NO_2 concentrations and population density patterns.

To evaluate the relationship between NO_2 concentrations and population density, Pearson's correlation analysis was conducted using seasonal and annual mean NO_2 data for the period 2022–2024. The analysis was limited to land-based grid cells (inland and coastal zones) where population data from the 2021 national census could be spatially matched with the NO_2 dataset [28].

Because the spatial resolution of the census data and the NO_2 grids differed, population counts were first converted from administrative raster units into point features representing population-weighted centroids. These points were then spatially overlaid onto the NO_2 grid using GIS-based techniques to compute the total number of residents within each NO_2 grid cell. This method enabled integration of the two datasets despite the original grid mismatch and allowed for consistent spatial alignment.

Although population data represented the year 2021 and NO_2 data spanned 2022–2024, the spatial distribution of residents was assumed to remain stable over this short interval. The temporal offset was considered a minor limitation and did not substantially affect the validity of spatial association analyses.

Correlation coefficients were calculated separately for surface-level (0 m) and elevated (50 m) NO_2 concentrations, allowing for altitude-specific interpretation of population exposure. Seasonal correlations (winter, spring, summer, and autumn) and aggregated annual correlations were used to identify both consistent and seasonally variable spatial associations.

3. Results

3.1. Land–Sea Gradients in NO_2 Concentration

Approximately 40% of the world's population lives within 100 km of the coastline [29], and coastal zones often host multiple overlapping sources of nitrogen dioxide (NO_2) emissions—such as road transport, port operations, and maritime shipping. Numerous studies have investigated spatial NO_2 differences between land and sea environments, aiming to understand the role of maritime activity in shaping coastal air pollution patterns. Some of these studies, particularly in heavily trafficked regions such as East Asia, have identified elevated NO_2 concentrations along major shipping corridors, extending far offshore and exhibiting clear spatial structures [30]. Other studies have focused on broader land–sea contrasts, consistently reporting that NO_2 concentrations tend to be lower over oceanic areas compared to land, where emission sources are more concentrated [31]. Our results support these broader findings. Over the 2022–2024 period, average NO_2 concentrations were lower in offshore areas (3.53 ppmv) than in inland areas (4.20 ppmv), with a mean difference of -0.67 ppmv. Moreover, consistent with studies from high-traffic maritime zones, our data show that certain offshore areas near the Lithuanian coast exhibit elevated NO_2 concentrations—highlighting the most actively navigated parts of the regional marine environment (Figure 3).

As shown in Figure 3, the highest annual NO_2 concentrations were consistently observed in the “d-” group grid cells (1d-, 2d-, 3d-, and 4d-) across all years from 2022 to 2024, with values markedly exceeding the general offshore background of approximately 3.5 ppmv. In 2022, concentrations ranged from 2.94 ppmv in 4d- to 5.51 ppmv in 1d-, corresponding to excess levels of 0 to 2.01 ppmv above background. In 2023, concentrations

increased slightly, ranging from 3.48 ppmv in 4d- to 5.67 ppmv in 2d-, representing an excess of 0.03 to 2.17 ppmv. The most significant rise occurred in 2024, with concentrations ranging from 7.18 ppmv in 4d- to 9.01 ppmv in 1d-, and respective exceedances of 3.68 to 5.51 ppmv.

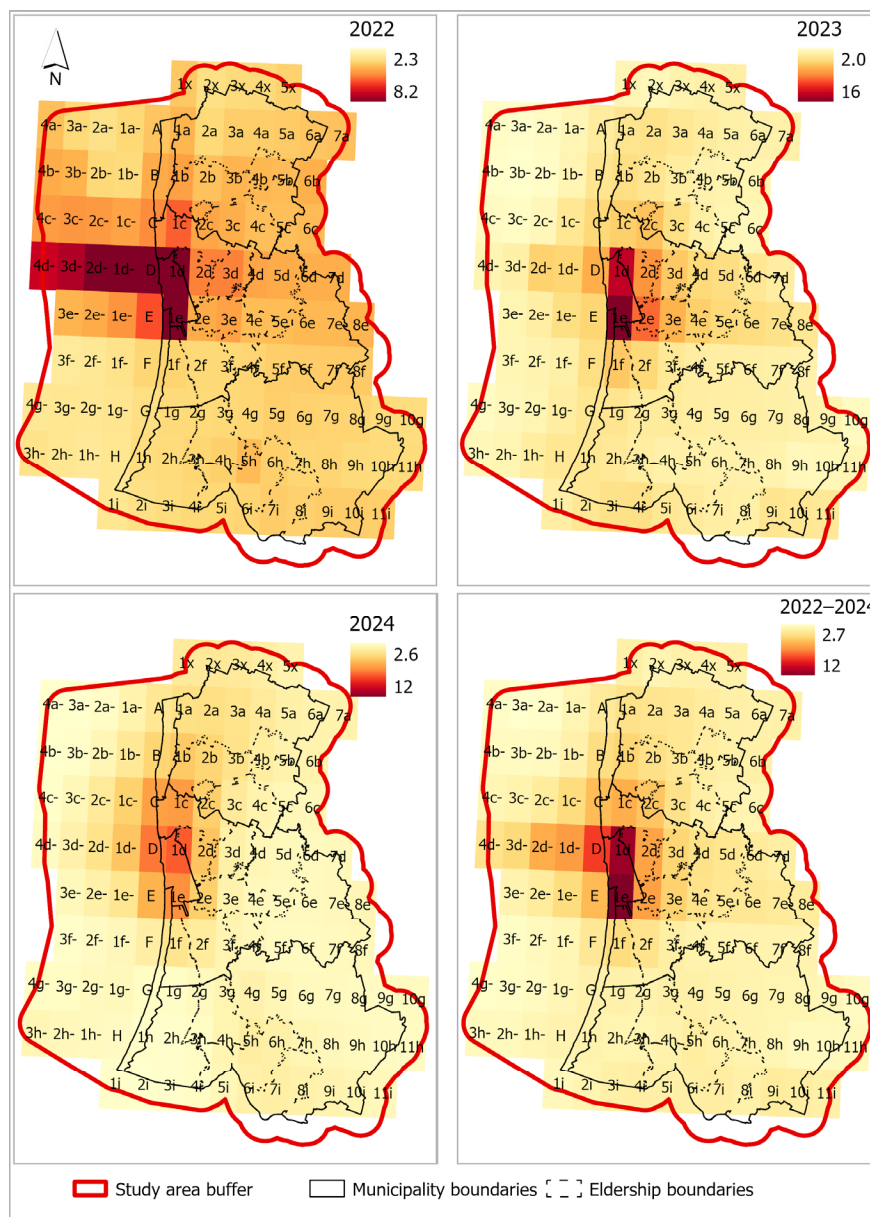


Figure 3. Annual mean NO₂ concentrations (ppmv) 2022–2024.

This consistent pattern indicates a strong year-on-year increase in NO₂ levels, with a growing divergence from the offshore background in each successive year. When averaged over the entire period, concentrations in the d-group cells ranged from 4.53 to 6.68 ppmv, equivalent to a persistent and localized enhancement of 1.03 to 3.18 ppmv above the marine baseline. These findings highlight both a temporally intensifying and spatially stable NO₂ anomaly within this coastal zone. In addition, several adjacent cells from the “c-” and “e-” groups also showed moderately elevated concentrations during the 2022–2024 period. Although their absolute values were lower than in the d-cells, they frequently exceeded the offshore background by up to 1.5–2 ppmv, particularly in 2023 and 2024. This further reinforces the spatial coherence of the observed anomaly and suggests a broader

influence zone. These elevated d-, c-, and e- cells are located in the marine area west of Klaipėda—Lithuania’s largest port and a key industrial and transport hub—indicating a likely contribution from shipping-related emissions in nearshore waters, potentially associated with vessel approach lanes, anchorage areas, or maneuvering zones.

While distinct NO₂ hotspots were observed near Klaipėda, particularly in the “d-” grid section, a clear offshore decrease in concentrations—from 1d- to 4d—was also evident. This observed local gradient provided the rationale for a broader analysis to assess whether a similar relationship between NO₂ levels and distance from the coastline exists across the full Lithuanian marine sector. However, when this relationship was examined at a broader spatial scale, encompassing the full offshore area, no consistent pattern of decreasing NO₂ concentrations with increasing distance from the coastline was observed (Table 1). This result was supported by statistical analysis using the Pearson correlation method. Pearson correlation coefficients (*r*) were calculated between grid cell distance from the coastline and annual mean NO₂ concentrations. Correlations were computed separately for each year (2022, 2023, and 2024), at two vertical levels (0 m and 50 m), and independently for the seaward (offshore) and landward (inland) zones. The inclusion of both surface-level and elevated measurements enabled the examination of potential vertical differences in spatial patterns, accounting for the effects of atmospheric mixing.

Table 1. Pearson correlation coefficients (*r*) between annual mean NO₂ concentrations and distance from the coastline.

	Spatial Area	Altitude (m)	Pearson <i>r</i>	<i>p</i> -Value	95% CI (Δ)
2022	Offshore	0	−0.345	0.0528	[−0.619, 0.004]
2022	Inland–full	0	−0.502	<0.001	[−0.658, −0.304]
2022	Inland <i>n</i> -32	0	−0.525	0.0020	[−0.739, −0.216]
2022	Offshore	50	−0.352	0.0481	[−0.624, −0.004]
2022	Inland–full	50	−0.451	<0.001	[−0.619, −0.243]
2022	Inland <i>n</i> -32	50	−0.512	0.0027	[−0.730, −0.199]
2023	Offshore	0	0.007	0.9715	[−0.343, 0.355]
2023	Inland–full	0	−0.228	0.0560	[−0.438, 0.006]
2023	Inland <i>n</i> -32	0	−0.349	0.0504	[−0.622, −0.000]
2023	Offshore	50	0.085	0.6421	[−0.272, 0.421]
2023	Inland–full	50	−0.201	0.0932	[−0.415, 0.034]
2023	Inland <i>n</i> -32	50	−0.332	0.0632	[−0.610, 0.019]
2024	Offshore	0	−0.007	0.9699	[−0.355, 0.343]
2024	Inland–full	0	−0.330	0.0050	[−0.523, −0.105]
2024	Inland <i>n</i> -32	0	−0.415	0.0181	[−0.667, −0.078]
2024	Offshore	50	0.007	0.9682	[−0.343, 0.355]
2024	Inland–full	50	−0.276	0.0199	[−0.478, −0.046]
2024	Inland <i>n</i> -32	50	−0.345	0.0531	[−0.619, 0.004]
2022–2024	Offshore	0	−0.094	0.6099	[−0.429, 0.263]
2022–2024	Inland–full	0	−0.338	0.0039	[−0.530, −0.114]
2022–2024	Inland <i>n</i> -32	0	−0.429	0.0143	[−0.676, −0.094]
2022–2024	Offshore	50	−0.060	0.7461	[−0.400, 0.295]
2022–2024	Inland–full	50	−0.302	0.0105	[−0.500, −0.074]
2022–2024	Inland <i>n</i> -32	50	−0.399	0.0236	[−0.656, −0.058]

The results revealed markedly different trends between the landward and seaward zones. In the offshore domain, the relationship between NO₂ concentrations and distance from the coastline was inconsistent and generally statistically insignificant. Only in 2022 was a weak-to-moderate negative correlation observed—approaching significance at 0 m ($r = -0.345$, $p = 0.0528$) and reaching significance at 50 m ($r = -0.352$, $p = 0.0481$). However, this trend did not persist in subsequent years. In both 2023 and 2024, correlation coefficients

were near zero, and p -values exceeded conventional thresholds, indicating the absence of a stable offshore gradient. Analysis of the three-year mean (2022–2024) also failed to identify any statistically significant relationship, suggesting that the 2022 result likely reflects short-term variability rather than a persistent spatial pattern.

By contrast, inland grid cells exhibited a more consistent and interpretable spatial structure. In 2022, strong and statistically significant negative correlations were detected at both altitudes ($r = -0.502$ at 0 m, $r = -0.451$ at 50 m; both $p < 0.001$), clearly indicating that NO_2 concentrations decreased with increasing distance inland. Although these relationships weakened in 2023—with correlation coefficients falling and p -values reaching marginal significance ($r = -0.228$ at 0 m, $p = 0.0560$; $r = -0.201$ at 50 m, $p = 0.0932$)—a spatial trend remained detectable. This may reflect interannual variation in meteorological conditions or emission distribution. In 2024, the inland gradient re-emerged, with moderate but statistically significant correlations ($r = -0.330$ at 0 m, $p = 0.0050$; $r = -0.276$ at 50 m, $p = 0.0199$). The three-year average analysis confirmed the persistence of this inland trend, with statistically significant negative correlations at both heights ($r = -0.338$ at 0 m, $p = 0.0039$; $r = -0.302$ at 50 m, $p = 0.0105$), demonstrating that NO_2 concentrations generally declined inland from the coast.

To address the unequal sample sizes between inland ($n = 71$) and offshore ($n = 32$) zones, a control analysis was performed using a subset of 32 inland grid cells selected based on a fixed spatial sampling strategy. This allowed for a balanced comparison. The reduced-sample analysis confirmed that the inland gradient was not driven by sample size. In 2022, strong and statistically significant correlations persisted ($r = -0.525$ at 0 m, $p = 0.0020$; $r = -0.512$ at 50 m, $p = 0.0027$). In 2023, although the correlation coefficients were slightly stronger than in the full sample, statistical significance remained borderline ($p \approx 0.05$ – 0.06), likely reflecting reduced statistical power. In 2024, the correlation at 0 m remained significant ($p = 0.0181$), while the 50 m value approached significance ($p = 0.0531$). The three-year average correlations in the reduced inland sample also remained statistically significant at both heights ($p < 0.05$), further supporting the robustness of the inland NO_2 gradient (Table 1).

These results reveal a clear contrast between inland and marine (offshore) NO_2 distribution patterns. While the inland zone consistently exhibited a negative correlation between NO_2 concentrations and distance from the coastline over the 2022–2024 period—a directional decrease in concentrations moving inland—no comparable trend was detected in the offshore domain. Although no consistent, region-wide offshore gradient was observed, a localized and spatially stable NO_2 enhancement was clearly expressed in the western coastal area near Klaipėda—Lithuania’s principal seaport.

This contrast reflects fundamental differences in emission geography between land and sea. On land, a large share of anthropogenic sources (settlements, road networks, and industry) forms a spatially continuous emission field and is often concentrated in coastal regions; globally, it is widely reported that around 40% of the world’s population lives within 100 km of the coastline. In the marine environment, by contrast, there is no analogous land-based emission structure. Offshore NO_2 patterns are shaped primarily by localized maritime sources and dispersion—particularly shipping lanes, port approach corridors, and potential anchorage areas—meaning that distance from the coastline is not the primary organizing factor of the spatial structure.

3.2. Vertical Structure and Seasonal Variability of NO_2

In the previous sections, we analyzed the horizontal distribution of NO_2 over land and sea. However, to comprehensively assess pollutant dynamics, it is also essential to consider their vertical structure within the lower atmospheric layers. Even within a relatively narrow

altitude range (0–50 m), vertical concentration differences can reveal important atmospheric properties, such as layer stability and vertical mixing efficiency, which determine whether pollutants tend to accumulate or disperse near the surface [32].

Previous studies have shown that in urbanized areas, atmospheric stratification is often more pronounced due to increased surface roughness, anthropogenic heat fluxes, and high emission densities. These factors enhance atmospheric stability and suppress vertical dispersion, leading to pollutant accumulation within lower layers. For example, a study conducted in Basel, Switzerland found that under stable atmospheric conditions, NO₂ concentrations between 30 and 70 m were consistently higher than those near ground level [32]. In contrast, the marine environment typically exhibits weaker atmospheric stability due to more uniform surface temperatures, lower anthropogenic influence, and stronger air exchange. As a result, vertical gradients in NO₂ concentrations tend to be weak or absent over open sea areas [33].

Due to these contrasts, the coastal zone emerges as a particularly important area of study. It represents a transitional environment where different emission sources and atmospheric regimes converge. Coastal areas are influenced by both terrestrial sources such as transport, urbanization and marine sources, while meteorological conditions vary rapidly and heterogeneously. Such variations are driven by changing synoptic and mesoscale processes, including land–sea breezes, which generate significant fluctuations in pressure gradients, wind direction, and turbulence [34]. Seasonal changes further amplify these dynamics, as vertical mixing, boundary layer height, and thermal stratification differ considerably between seasons—thereby influencing the extent to which pollutants accumulate or disperse in coastal environments. Figure 4 presents a synthesized visual summary of vertical NO₂ concentration differences across offshore, coastal, and inland zones in the Lithuanian coastal region, based on data from the 2022–2024 period.

The data are aggregated over the 2022–2024 period to emphasize stable seasonal patterns and reduce interannual variability. Each panel illustrates the seasonal distribution of station-level vertical NO₂ differences, while triangular markers indicate the arithmetic mean of the seasonally aggregated differences for each domain. To support the seasonal and spatial patterns illustrated in Figure 4, Table 2 presents key statistical estimates, including 95% confidence intervals and Cohen’s *d*z effect sizes. These metrics confirm that the observed vertical gradients are not only visually evident but also statistically robust and consistent across domains.

The results demonstrate a clear and consistent seasonal modulation of vertical NO₂ gradients across all spatial domains. The strongest vertical differentiation was observed during autumn. In this season, the mean vertical difference reached 1.116 ppmv in the coastal transition zone, 0.910 ppmv in the full inland domain, 0.867 ppmv in the reduced inland subset, and 0.837 ppmv in the offshore domain. These mean values are supported by the statistical analysis presented in Table 2. In the coastal transition zone, the autumn mean difference of 1.116 ppmv was associated with a 95% confidence interval of 0.898–1.333 ppmv and a very large effect size (Cohen’s *d*z = 4.29). In the full inland domain, the corresponding mean of 0.910 ppmv had a 95% confidence interval of 0.880–1.013 ppmv and an effect size of *d*z = 3.38, while the reduced inland subset exhibited a mean of 0.867 ppmv with a 95% confidence interval of 0.741–0.992 ppmv and *d*z = 2.50. Offshore, the autumn mean difference of 0.837 ppmv was associated with a 95% confidence interval of 0.575–1.023 ppmv and an effect size of *d*z = 1.29. Together, these results indicate strong and statistically robust vertical stratification during autumn across all domains. The wider autumn interquartile ranges (Figure 4) can be related to alternating boundary-layer mixing regimes during this transitional season—ranging from stable, weak-mixing conditions that promote near-surface pollutant accumulation to windy, well-mixed situations that reduce

stratification. Such behavior is consistent with findings by Seidel [35], who reported that autumn in Europe is often characterized by reduced planetary boundary layer heights and enhanced atmospheric stability, conditions that promote vertical pollutant accumulation.

Table 2. Correlation analysis of annual and seasonal NO₂ variability across offshore, coastal, and inland domains for the 2022–2024 period.

Season	Spatial Area	<i>n</i>	Pearson <i>r</i>	<i>p</i> -Value	95% CI (Δ)	Cohen (<i>dz</i>)
Annual	Offshore	32	0.988	<0.001	[0.224, 0.335]	1.82
Annual	Coastline	8	0.999	<0.001	[0.270, 0.472]	3.07
Annual	Land (inland)	71	0.997	<0.001	[0.420, 0.500]	2.75
Annual	Land (inland)– <i>n</i> = 32	32	0.998	<0.001	[0.391, 0.563]	2.0
Winter	Offshore	32	1.0	<0.001	[0.010, 0.029]	0.73
Winter	Coastline	8	1.0	<0.001	[0.018, 0.042]	2.11
Winter	Land (inland)	71	0.999	<0.001	[0.085, 0.104]	2.34
Winter	Land (inland)– <i>n</i> = 32	32	0.999	<0.001	[0.073, 0.112]	1.7
Spring	Offshore	32	0.996	<0.001	[0.131, 0.220]	1.41
Spring	Coastline	8	0.999	<0.001	[0.060, 0.291]	1.27
Spring	Land (inland)	71	0.998	<0.001	[0.298, 0.409]	1.51
Spring	Land (inland)– <i>n</i> = 32	32	0.997	<0.001	[0.354, 0.576]	1.51
Summer	Offshore	32	0.997	<0.001	[0.050, 0.143]	0.74
Summer	Coastline	8	1.0	<0.001	[0.048, 0.202]	1.36
Summer	Land (inland)	71	0.997	<0.001	[0.349, 0.459]	1.73
Summer	Land (inland)– <i>n</i> = 32	32	0.998	<0.001	[0.325, 0.558]	1.37
Autumn	Offshore	32	0.657	<0.001	[0.575, 1.023]	1.29
Autumn	Coastline	8	0.994	<0.001	[0.898, 1.333]	4.29
Autumn	Land (inland)	71	0.982	<0.001	[0.880, 1.013]	3.38
Autumn	Land (inland)– <i>n</i> = 32	32	0.99	<0.001	[0.741, 0.992]	2.5

In contrast, winter exhibited the weakest vertical NO₂ gradients throughout the study area. Mean vertical differences during winter amounted to 0.019 ppmv in the offshore domain, 0.030 ppmv in the coastal transition zone, 0.095 ppmv in the full inland domain, and 0.092 ppmv in the reduced inland subset. These values were associated with 95% confidence intervals of 0.010–0.029 ppmv offshore, 0.018–0.042 ppmv in the coastal zone, 0.085–0.104 ppmv in the full inland domain, and 0.073–0.112 ppmv in the reduced inland subset. Corresponding effect sizes were smaller than in autumn, with Cohen’s *dz* = 0.73 offshore, 2.11 in the coastal transition zone, 2.34 inland, and 1.70 in the reduced inland subset. Although all paired *t*-tests indicated statistically significant differences (*p* < 0.001), the small magnitudes of the mean differences reflect weak vertical stratification during winter, consistent with enhanced mechanical mixing, stronger winds, and a lower frequency of persistent inversion conditions [36].

Spring and summer exhibited intermediate vertical differentiation. During spring, the mean vertical difference reached 0.175 ppmv offshore, 0.176 ppmv in the coastal transition zone, 0.354 ppmv in the full inland domain, and 0.465 ppmv in the reduced inland subset. These values were supported by 95% confidence intervals of 0.131–0.220 ppmv offshore, 0.060–0.291 ppmv in the coastal zone, 0.298–0.409 ppmv in the full inland domain, and 0.354–0.576 ppmv in the reduced inland subset. Effect sizes during spring were moderate and consistent across domains, with Cohen’s *dz* = 1.41 offshore, 1.27 in the coastal transition zone, 1.51 in the full inland domain, and 1.51 in the reduced inland subset. These results indicate a stable and spatially coherent springtime vertical structure, likely associated with increasing atmospheric stability during the seasonal transition.

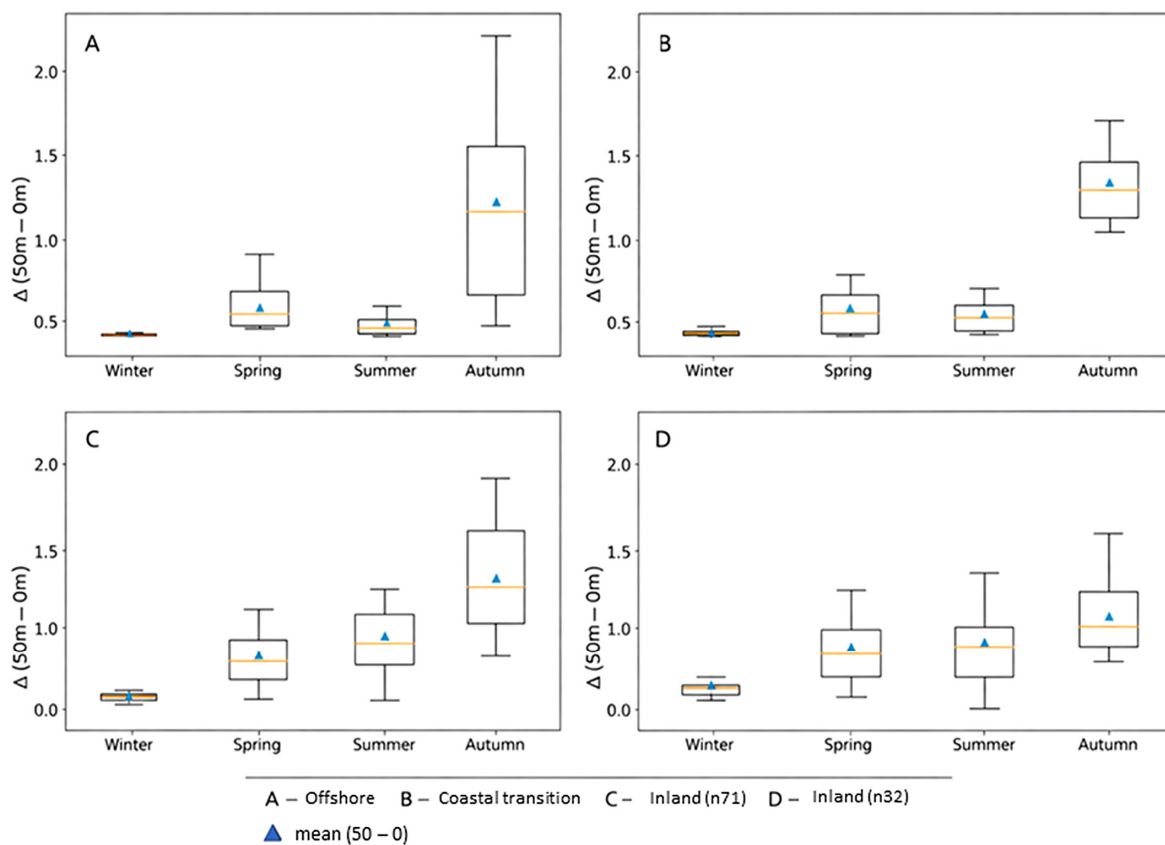


Figure 4. Seasonal paired mean differences in NO_2 concentrations between 50 m and 0 m heights across geographical domains during 2022–2024. Boxplots show $\Delta(\text{NO}_2) = \text{NO}_2_{[50\text{ m}]} - \text{NO}_2_{[0\text{ m}]}$ for offshore (A), coastal transition (B), inland ($n = 71$; (C)), and reduced inland ($n = 32$; (D)). In each boxplot, the central horizontal line indicates the median, the box represents the interquartile range, the whiskers indicate the data range, and the blue triangle marks the mean value.

During summer, the mean vertical difference amounted to 0.096 ppmv offshore, 0.125 ppmv in the coastal transition zone, 0.404 ppmv in the full inland domain, and 0.441 ppmv in the reduced inland subset. The corresponding 95% confidence intervals were 0.050–0.143 ppmv offshore, 0.048–0.202 ppmv in the coastal transition zone, 0.349–0.459 ppmv in the full inland domain, and 0.325–0.558 ppmv in the reduced inland subset. Effect sizes during summer remained substantial over land, with Cohen's $d_z = 1.73$ in the full inland domain and 1.37 in the reduced inland subset, while offshore and coastal effect sizes were 0.74 and 1.36, respectively. These findings indicate that pronounced vertical NO_2 gradients persist over land even under conditions of enhanced convective mixing.

To assess the spatial coherence of vertical NO_2 gradients, Pearson correlation coefficients were calculated between annual mean NO_2 concentrations at 0 m and 50 m for each domain. Across all domains and years, very strong positive correlations were observed, with Pearson correlation coefficients exceeding 0.98 ($p < 0.001$). This indicates that locations with elevated surface-level NO_2 concentrations also consistently exhibited higher concentrations at 50 m, demonstrating that both heights respond to the same emission sources and regional atmospheric processes. Consequently, the observed vertical differences primarily reflect atmospheric structure and mixing conditions rather than independent source contributions.

In summary, the results show that vertical NO_2 gradients in the Lithuanian coastal region exhibit pronounced and robust seasonal behavior. The largest mean vertical differences occur during autumn, coinciding with enhanced atmospheric stability, while winter is

characterized by minimal vertical stratification. Spring and summer represent intermediate conditions, with persistent but weaker gradients. The consistency of mean values, large and well-defined effect sizes, non-overlapping confidence intervals, and strong vertical correlations collectively confirm that the observed vertical NO₂ differences represent a statistically robust and physically meaningful feature of near-surface air quality dynamics in coastal and inland environments.

3.3. Surface NO₂ Distributions in Relation to Population Density Gradients

Many studies have demonstrated that the spatial distribution of NO₂ is closely linked to human activity in urbanised areas. Road transport is the primary source of NO₂ in Europe, while combustion processes in industry and the energy sector also make substantial contributions. Consequently, the highest NO₂ concentrations are typically observed in densely populated, high-traffic environments [37]. This pattern is also evident along the Lithuanian coast, where NO₂ and particulate matter hotspots in the port city of Klaipėda are strongly associated with traffic flows, port-related and urban functions, and demographic concentration [38,39].

To contextualise these pollution patterns, the spatial distribution of the population along the Lithuanian coastline was examined as a key proxy for the intensity of urban activity and related emission sources. The results reveal a pronounced demographic concentration within a narrow coastal belt. The coastal interface zone is represented by grid cells located directly along the shoreline (A–I), while the adjacent first inland belt is captured by grid cells 1a–1i (Figure 2). Together, these two neighbouring belts (A–I; 1a–1i) extend approximately 12.4 km inland from the coast, based on the CAMS Copernicus grid step, which is about 6.2 km at Lithuanian latitudes [40]. This area accommodates around 161,789 inhabitants, or 54.2% of the study area's total population. The remaining inland territory beyond this belt holds 136,732 individuals, or 45.8%.

To better represent the full spatial extent of coastal demographic influence—including the suburbanized periphery of Klaipėda city and settlements along the Curonian Lagoon—an extended zone was delineated by including grid cells 2a–2i. This broader belt reaches up to approximately 18.6 km from the coast and increases the total coastal population to 215,096, or 72.1% of the study area's population. These results indicate that demographic dominance is concentrated in the coastal region, not only along the immediate seafront but also across a functionally connected hinterland.

This demographic pattern is consistent with broader spatial trends observed across the European Union, where coastal regions tend to concentrate population and urban functions. Eurostat reports that in 2007, 43% of the population of the 22 EU Member States with a sea border lived in coastal regions, and 38% of coastal-region inhabitants resided in one of 194 cities with more than 100,000 inhabitants located within 50 km of the sea [41]. The reported proportions indicate that coastal population dominance is not confined to the immediate shoreline, but extends into an urbanised, functionally connected coastal hinterland.

This population pattern closely mirrors spatial trends in nitrogen dioxide (NO₂) concentrations. Based on aggregated data from 2022 to 2024, total NO₂ loads were calculated by averaging surface-level (0 m) and near-surface (50 m) measurements across all grid cells and time periods. The results show that the combined area of A–I and 1a–1i grids—extending 12.4 km inland—accounted for approximately 52.6% of the total NO₂ burden in the study area. Notably, the inland portion (1a–1i) contributed the majority of this share, at 46.4%, while the immediate coastal interface (A–I) contributed only 6.2%.

Expanding the analysis to include grid cells 2a–2i—representing the broader coastal hinterland up to 18.6 km inland—reveals an additional 19.5% of the total NO₂ load. In

total, the coastal and near-coastal zone (A–I, 1a–1i, and 2a–2i) generated 72.1% of all NO₂ emissions measured across the study area during the 2022–2024 period.

Within this coastal zone, the Klaipėda urban grid cells (D, E, 1d, and 1e) constitute a particularly significant emission hotspot, contributing approximately 27.4% of the total coastal NO₂ load. This indicates that over one-quarter of the nitrogen dioxide accumulated in the coastal belt originates from the Klaipėda metropolitan area—the largest urban and industrial center on the Lithuanian coast.

These results clearly indicate that NO₂ accumulation is concentrated not directly at the shoreline but primarily in densely populated and urbanized inland zones near the coast, particularly around Klaipėda’s metropolitan region. This pattern reflects the influence of anthropogenic activities—including traffic, industry, and dense residential development—on atmospheric pollutant distribution in coastal environments.

To further examine the relationship between population density and NO₂ distribution, a correlation analysis was conducted across all grid cells in the study area. This statistical approach complements the spatial findings by assessing the strength of association between population size and NO₂ concentration at two vertical levels (0 m and 50 m), both seasonally and annually. The resulting patterns are presented in Figure 5.

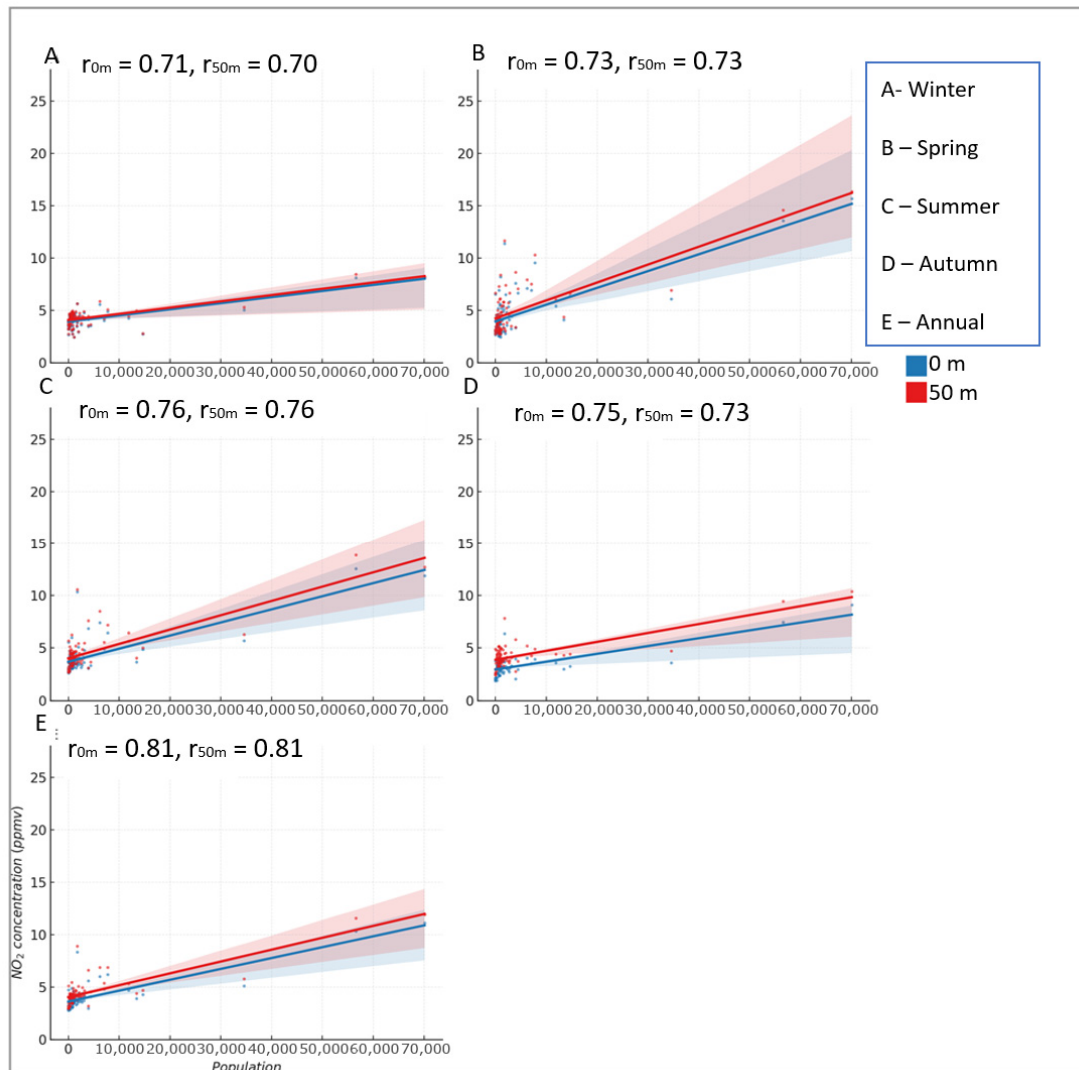


Figure 5. Correlations between population and mean NO₂ concentration at two heights (0 m and 50 m) during 2022–2024. (A) Winter, (B) Spring, (C) Summer, (D) Autumn, (E) Annual. Blue lines indicate 0 m, red lines indicate 50 m, and shaded areas represent 95% confidence intervals.

The plotted results (Figure 5) demonstrate a clear and consistent positive association between population size and nitrogen dioxide (NO₂) concentrations across all seasons and both measurement heights. In each seasonal group (winter, spring, summer, autumn) and in the annual average, linear regression models illustrate the trend lines for 0 m (blue) and 50 m (red) above sea level. The shaded areas indicate 95% confidence intervals, showing the range within which the true relationship is likely to fall. Together, these visual patterns provide the basis for interpreting how NO₂ concentrations vary with population density across different seasons and altitudes.

The annual relationship between population and NO₂ concentration demonstrates the strongest correlation across all datasets, with a Pearson coefficient of $r = 0.81$ observed at both measurement heights. This finding suggests that NO₂ accumulation is not merely a seasonal phenomenon but a persistent feature of densely populated areas. It reflects the continuous impact of human-induced emissions such as traffic, residential heating, and industrial activities on local air quality throughout the year.

Among the seasonal trends, the summer correlation is notably strong ($r = 0.76$ at both 0 m and 50 m), and the regression lines display high consistency across the population gradient. This pattern likely reflects the dominant role of traffic-related emissions during the warmer months, when residential heating is absent. Evidence from land-use regression modelling supports this interpretation, as traffic-related predictors are often among the most influential variables explaining NO₂ spatial variability [42].

The correlation is slightly weaker in winter ($r = 0.71 - 0.70$), autumn ($r = 0.75 - 0.73$), and spring ($r = 0.73$), despite elevated NO₂ levels during colder periods. This can be attributed to a combination of seasonal atmospheric conditions and additional heating-related emissions that vary in intensity and spatial distribution. Reduced solar radiation in winter slows photochemical processing of NO₂, while lower temperatures increase heating-related emissions, contributing to higher concentrations during the cold season [43]. In addition, residential combustion can introduce spatially heterogeneous NO₂ contributions, particularly where individual heating systems and solid fuels are used, which can weaken the alignment between NO₂ and population density compared with summer conditions [44]. Spring exhibits a transitional pattern ($r = 0.73$), consistent with declining heating demand and a gradual return to a stronger relative dominance of mobile sources.

The analysis confirms a strong and consistent association between population density and NO₂ concentration across all seasons and altitudes. The strongest relationship is observed in the annual dataset ($r = 0.81$), which is based on a larger number of observations and therefore provides the clearest evidence of a particularly strong association between population density and NO₂ concentration. This consistency across seasonal contexts indicates that anthropogenic pressure, particularly from transport and residential energy use, is the dominant factor shaping NO₂ distribution patterns in the Lithuanian coastal region.

4. Conclusions and Discussion

This study provides a comprehensive assessment of nitrogen dioxide (NO₂) distribution patterns in Lithuania's coastal (including adjacent municipalities representing the regional NO₂ background) and marine environment during the 2022–2024 period. The results demonstrate that spatial variability in NO₂ concentrations across this region is shaped by the combined influence of anthropogenic emission sources, atmospheric dispersion processes, and vertical structure. Although the analysis is based on a relatively short three-year period, the recurrence of the identified spatial patterns across all study years suggests the presence of consistent tendencies rather than isolated or random events.

When interpreting the reported NO₂ patterns, potential differences in representativeness and precision between urbanized land areas and coastal/marine grid cells should be

considered. Over strongly urbanized zones, concentration fields may capture robust spatial gradients driven by dense emission sources, but the 0.1° grid resolution can smooth sharp near-source variability and underestimate local extremes. In coastal settings, additional uncertainty may arise from the land–sea transition within grid cells, shoreline complexity, and meteorology-driven retrieval/assimilation constraints (cloudiness and changing boundary-layer conditions), which can affect the stability of nearshore estimates. For these reasons, the present results are interpreted primarily in terms of consistent spatial gradients and recurrent hotspot structures (relative differences) rather than exact point-level concentrations. With these interpretative considerations in mind, the analysis first contrasts marine and land areas and then examines the location and persistence of NO_2 hotspots.

Mean NO_2 concentrations over marine areas were consistently lower than those observed over land, in agreement with previous studies indicating that dominant NO_2 emission sources are primarily terrestrial. However, a more detailed analysis of marine grid cells revealed that NO_2 distribution over the sea is not spatially homogeneous. Instead, distinct localized zones of elevated concentrations—hereafter referred to as NO_2 “hotspots”—were identified and found to be closely associated with areas of intensive human activity. These elevated concentration zones are aligned parallel to Lithuania’s largest coastal city and port, Klaipėda, with NO_2 levels gradually decreasing with increasing distance offshore, reflecting the combined influence of localized emission sources and atmospheric dispersion processes.

The most pronounced and spatially persistent NO_2 hotspots were detected within the “d-” group marine grid cells (1d-, 2d-, 3d-, and 4d-), where concentrations consistently exceeded the general offshore background throughout the study period. NO_2 levels in these cells remained systematically higher than in adjacent marine areas, and an increasing concentration tendency was observed during 2023–2024. Moderately elevated concentrations were also identified in neighboring “c-” and “e-” grid groups, particularly in the later years of the analysis, suggesting the presence of a broader emission-influenced zone. The spatial location of these anomalies west of the Port of Klaipėda indicates a likely contribution from shipping-related activities, including vessel maneuvering, anchorage, and port approach routes.

Although NO_2 levels in the identified hotspot corridor west of Klaipėda generally decrease with increasing distance offshore, this nearshore-to-offshore pattern is not universal across the entire Lithuanian marine sector. Distance to the coastline explains the gradient locally where a clear source region is present, but a broader sector-wide assessment does not show a consistent or statistically significant coastline-distance relationship. This interpretation is consistent with previous satellite-based evidence showing that over European seas marine NO_2 enhancements frequently occur as narrow, lane-like features associated with shipping corridors, rather than forming a smooth monotonic gradient with distance to the coastline [42]. This indicates that marine NO_2 patterns are primarily controlled by localized emission footprints (port-approach activity, maneuvering/anchorage areas, and major shipping routes) and by short-term transport and dispersion conditions (wind direction and speed, turbulence, and boundary-layer mixing), which can shift and dilute NO_2 independently of shoreline distance.

Vertical analysis revealed systematic differences in NO_2 concentrations between the 0 m and 50 m height levels, particularly in autumn and over land areas, suggesting that periods of increased atmospheric stability and boundary-layer stratification may enhance pollutant accumulation near the surface. At the same time, the very strong correlation between NO_2 concentrations at both heights across all analyzed years indicates that the pollution signal at these levels is controlled by the same emission sources and regional

atmospheric processes. Consequently, the main spatial patterns of NO₂ distribution remain consistent throughout this vertical interval.

Several limitations of this study should be acknowledged. The three-year study period does not allow for a robust assessment of long-term trends or structural stability under broader climatic variability. In addition, the lack of high-resolution meteorological data limited the ability to directly link observed NO₂ structures to specific atmospheric processes such as wind regimes, inversion strength, or boundary-layer height. Nevertheless, the repeated occurrence of the identified NO₂ hotspots across all study years suggests that these features are not episodic, although longer observation periods are required to confirm their long-term persistence.

The results of this study indicate that NO₂ distribution in Lithuania's coastal (including adjacent municipalities representing the regional NO₂ background) and marine environment is shaped not only by gradual spatial gradients but also by distinct, spatially coherent zones of elevated concentrations closely associated with human activity. The spatial coincidence of these NO₂ hotspots with intensively urbanized and functionally important coastal areas highlights the need to consider air pollution patterns as an integral component of coastal urban systems. Remote sensing-based assessment of NO₂ distribution provides a valuable tool for identifying areas of elevated pollution not only over land but also in marine environments where conventional monitoring is often limited. Such spatially explicit information can support more sustainable coastal urban planning by helping to better align urban development, transport infrastructure, and environmental protection objectives.

Author Contributions: Conceptualization, A.A.; methodology, A.A.; software, A.A.; R.D. and E.V.; investigation, A.A. and E.V., writing and editing, A.A. and I.D.; visualization, A.A. and E.V.; supervision, I.D. All authors have read and agreed to the published version of the manuscript.

Funding: This research received no external funding.

Institutional Review Board Statement: Not applicable.

Informed Consent Statement: Not applicable.

Data Availability Statement: The data presented in this study are available on request from the corresponding author.

Conflicts of Interest: The authors declare no conflicts of interest.

References

1. Mucha, W.; Mainka, A. Exposure to Nitrogen Dioxide (NO₂) Emitted from Traffic-Related Sources. *Appl. Sci.* **2026**, *16*, 859. [[CrossRef](#)]
2. European Environment Agency (EEA). *Air Quality in Europe—2022 Report*; EEA Report No. 13/2022; European Environment Agency (EEA): Copenhagen, Denmark, 2022.
3. World Health Organization (WHO). *WHO Global Air Quality Guidelines: Particulate Matter (PM_{2.5} and PM₁₀), Ozone, Nitrogen Dioxide, Sulfur Dioxide and Carbon Monoxide*; World Health Organization (WHO): Geneva, Switzerland, 2021.
4. Beelen, R.; Stafoggia, M.; Raaschou-Nielsen, O.; Andersen, Z.J.; Ran, W.; Katsouyanni, K.; Dimakopoulou, K.; Brunekreef, B.; Weinmayr, G.; Hoffmann, B.; et al. Long-term exposure to air pollution and cardiovascular mortality: An analysis of 22 European cohorts. *Epidemiology* **2014**, *25*, 368–378. [[CrossRef](#)] [[PubMed](#)]
5. Veeffkind, J.P.; Aben, I.; McMullan, K.; Förster, H.; de Vries, J.; Otter, G.; Claas, J.; Eskes, H.J.; de Haan, J.F.; Kleipool, Q.; et al. TROPOMI on the ESA Sentinel-5 Precursor: A GMES mission for global observations of the atmospheric composition for climate, air quality and ozone layer applications. *Remote Sens. Environ.* **2012**, *120*, 70–83. [[CrossRef](#)]
6. Levelt, P.F.; Joiner, J.; Tamminen, J.; Veeffkind, J.P.; Bhartia, P.K.; Stein Zweers, D.C.; Duncan, B.N.; Streets, D.G.; Eskes, H.; van der A, R.; et al. The Ozone Monitoring Instrument: Overview of 14 years in space. *Atmos. Chem. Phys.* **2018**, *18*, 5699–5745. [[CrossRef](#)]

7. Lorente, A.; Boersma, K.F.; Eskes, H.J.; Veefkind, J.P.; van Geffen, J.H.G.M.; de Zeeuw, M.B.; Denier van der Gon, H.A.C.; Beirle, S.; Krol, M.C. Quantification of nitrogen oxides emissions from build-up of pollution over Paris with TROPOMI. *Sci. Rep.* **2019**, *9*, 20033. [[CrossRef](#)]
8. Prunet, P.; Lezeaux, O.; Camy-Peyret, C.; Thevenon, H. Analysis of the NO₂ tropospheric product from S5P TROPOMI for monitoring pollution at city scale. *City Environ. Interact.* **2020**, *8*, 100051. [[CrossRef](#)]
9. Liebuviėnė, L.; Čižiūnienė, L. *Strategic Development of the Port of Klaipėda*; Klaipėda University Press: Klaipėda, Lithuania, 2021.
10. Statistics Lithuania. *Territory, Administrative Units, and Population Statistics*; Statistics Lithuania: Vilnius, Lithuania, 2022.
11. HELCOM. *State of the Baltic Sea: Holistic Assessment*; HELCOM: Helsinki, Finland, 2018.
12. Kriauciūnienė, J.; Gailiušis, B.; Šarauskiėnė, D. Klimato kaitos įtakos Lietuvos vandens ištekliams tyrimai. *Energetika* **2016**, *62*, 23–33. [[CrossRef](#)]
13. Plotnikova, E.; Vienažindienė, M.; Slavinskas, S. Development of inland waterway transport as a key to ensure sustainability: A case study of Lithuania. *Sustainability* **2022**, *14*, 10532. [[CrossRef](#)]
14. Griffin, R.J.; Dabdub, D.; Kleeman, M.J.; Fraser, M.P.; Cass, G.R.; Seinfeld, J.H. Secondary organic aerosol 3. Urban/regional scale model of size- and composition-resolved aerosols. *J. Geophys. Res. Atmos.* **2002**, *107*, AAC-5. [[CrossRef](#)]
15. Galvonaitė, A.; Misiūnienė, M.; Valiukas, D.; Buitkuvienė, M.S. *Lietuvos Klimatas: Monografija*; Lietuvos Hidrometeorologijos Tarnyba: Vilnius, Lithuania, 2007.
16. Bossioli, E.; Tombrou, M.; Dandou, A. Planetary boundary-layer parameterizations in urban air quality over complex terrain. *Boundary-Layer Meteorol.* **2009**, *133*, 361–388.
17. EMSA. *European Maritime Safety Agency—Annual Overview 2020*; EMSA: Lisbon, Portugal, 2020.
18. Granier, C. CAMS global emissions. Presented at the CAMS-71 Project Presentation, Copernicus Atmosphere Monitoring Service, Brussels, Belgium, 12 March 2020.
19. Inness, A.; Ades, M.; Agustí-Panareda, A.; Barré, J.; Benedictow, A.; Blechschmidt, A.-M.; Dominguez, J.J.; Engelen, R.; Eskes, H.; Flemming, J.; et al. The CAMS reanalysis of atmospheric composition. *Atmos. Chem. Phys.* **2019**, *19*, 3515–3556. [[CrossRef](#)]
20. Cersosimo, A.; Serio, C.; Masiello, G. TROPOMI NO₂ Tropospheric Column Data: Regridding to 1 km Grid-Resolution and Assessment of their Consistency with In Situ Surface Observations. *Remote Sens.* **2020**, *12*, 2212. [[CrossRef](#)]
21. De Hoogh, K.; Saucy, A.; Shtein, A.; Schwartz, J.; West, E.; Strassmann, A.; Puhon, M.; Rössli, M.; Stafoggia, M.; Klotz, S.; et al. Predicting Fine-Scale Daily NO₂ for 2005–2016 Incorporating OMI Satellite Data Across Switzerland. *Environ. Sci. Technol.* **2019**, *53*, 10279–10287. [[CrossRef](#)] [[PubMed](#)]
22. Horálek, J.; Hamer, P.; Schreiberová, M.; Colette, A. *Potential Use of CAMS Modelling Results in Air Quality Mapping Under ETC/ATNI*; ETC/ATNI Report 2019/17; Zenodo: Geneva, Switzerland, 2019.
23. Longley, P.A.; Goodchild, M.F.; Maguire, D.J.; Rhind, D.W. *Geographic Information Systems and Science*, 4th ed.; Wiley: Chichester, UK, 2015.
24. United Nations. *United Nations Convention on the Law of the Sea (UNCLOS)*; United Nations: New York, NY, USA, 1982.
25. Dutilleul, P.; Stockwell, J.D.; Frigon, D. The Mantel test versus Pearson’s correlation analysis: Assessment of the differences for biological and environmental studies. *J. Agric. Biol. Environ. Stat.* **2000**, *5*, 131–150. [[CrossRef](#)]
26. Quinn, G.P.; Keough, M.J. *Experimental Design and Data Analysis for Biologists*; Cambridge University Press: Cambridge, UK, 2002.
27. Cumming, G.; Calin-Jageman, R.J. *The New Statistics: Why and How*; Routledge: New York, NY, USA, 2017.
28. Statistics Lithuania. *Population and Housing Census 2021*; Statistics Lithuania: Vilnius, Lithuania, 2021.
29. United Nations. *Percentage of Total Population Living in Coastal Areas*; UN Department of Economic and Social Affairs: New York, NY, USA, 2021.
30. Zhang, Y.; Li, R.; Fu, S.; Shi, M.; Han, Z.; Zhang, Y.; Chen, J. Driving factors of ship-induced nitrogen dioxide concentrations over coastal seas of China: Implications for ship emission management. *J. Environ. Manag.* **2025**, *373*, 123894. [[CrossRef](#)]
31. Adams, T.J.; Geddes, J.A.; Lind, E.S. New insights into the role of atmospheric transport and mixing on column and surface concentrations of NO₂ at a coastal urban site. *J. Geophys. Res. Atmos.* **2023**, *128*, e2022JD037704. [[CrossRef](#)]
32. Eeftens, M.; Odabasi, D.; Flückiger, B.; Davey, M.; Ineichen, A.; Feigenwinter, C.; Tsai, M.-Y. Modelling the vertical gradient of nitrogen dioxide in an urban area. *Sci. Total Environ.* **2019**, *650*, 452–458. [[CrossRef](#)]
33. Xing, C.; Xu, S.; Song, Y.; Liu, C.; Liu, Y.; Lu, K.; Tan, W.; Zhang, C.; Hu, Q.; Wang, S.; et al. A new insight into the vertical differences in NO₂ heterogeneous reaction to produce HONO over inland and marginal seas. *Atmos. Chem. Phys.* **2023**, *23*, 5815–5834. [[CrossRef](#)]
34. Seidel, D.J.; Ao, C.O.; Li, K. Estimating climatological planetary boundary layer heights from radiosonde observations: Comparison of methods and uncertainty analysis. *J. Geophys. Res. Atmos.* **2010**, *115*, D16. [[CrossRef](#)]
35. Stull, R.B. *An Introduction to Boundary Layer Meteorology*; Springer: Berlin/Heidelberg, Germany, 1988.
36. European Environment Agency. *Air Quality Status Report 2025: Nitrogen Dioxide (NO₂)*; European Environment Agency: Copenhagen, Denmark, 2025.

37. Andriulė, A.; Vasiliauskienė, E.; Rapalis, P.; Dailidienė, I. Air Pollution in the Port City of Lithuania: Characteristics of the Distribution of Nitrogen Dioxide and Solid Particles When Assessing the Demographic Distribution of the Population. *Sustainability* **2024**, *16*, 8413. [[CrossRef](#)]
38. Andriulė, A.; Suzdalev, S.; Vasiliauskienė, E.; Dailidienė, I. Air Pollution and Dispersion of Airborne Chemical Elements in Klaipėda Seaport-City. *Sustainability* **2025**, *17*, 3834. [[CrossRef](#)]
39. Copernicus Atmosphere Monitoring Service (CAMS). CAMS European air quality forecasts—Dataset description (horizontal resolution $0.1^\circ \times 0.1^\circ$, vertical levels incl. surface and 50 m). In *Atmosphere Data Store (ADS)*; Copernicus Atmosphere Monitoring Service (CAMS): Reading, UK, 2026.
40. Collet, I. *Portrait of EU Coastal Regions; Statistics in Focus, 38/2010; Catalogue No. KS-SF-10-038-EN-N*; Eurostat: Luxembourg, 2010; ISSN 1977-0316.
41. Riess, T.C.V.W.; Boersma, K.F.; van Vliet, J.; Peters, W.; Sneep, M.; Eskes, H.; van Geffen, J. Improved monitoring of shipping NO_2 with TROPOMI: Decreasing NO_x emissions in European seas during the COVID-19 pandemic. *Atmos. Meas. Tech.* **2022**, *15*, 1415–1438. [[CrossRef](#)]
42. Beelen, R.; Hoek, G.; Vienneau, D.; Eeftens, M.; Dimakopoulou, K.; Pedeli, X.; Tsai, M.-Y.; Künzli, N.; Schikowski, T.; Marcon, A.; et al. Development of NO_2 and NO_x land use regression models for estimating air pollution exposure in 36 study areas in Europe—The ESCAPE project. *Atmos. Environ.* **2013**, *72*, 10–23. [[CrossRef](#)]
43. Voiculescu, M.; Constantin, D.-E.; Condurache-Bota, S.; Călmuc, V.; Roșu, A.; Dragomir Bălănică, C.M. Role of Meteorological Parameters in the Diurnal and Seasonal Variation of NO_2 in a Romanian Urban Environment. *Int. J. Environ. Res. Public Health* **2020**, *17*, 6228. [[CrossRef](#)]
44. Plejdrup, M.S.; Nielsen, O.-K.; Brandt, J. Spatial emission modelling for residential wood combustion in Denmark. *Atmos. Environ.* **2016**, *144*, 389–396. [[CrossRef](#)]

Disclaimer/Publisher’s Note: The statements, opinions and data contained in all publications are solely those of the individual author(s) and contributor(s) and not of MDPI and/or the editor(s). MDPI and/or the editor(s) disclaim responsibility for any injury to people or property resulting from any ideas, methods, instructions or products referred to in the content.